Myc-driven murine prostate cancer shares molecular features with human prostate tumors

Katharine Ellwood-Yen,[1,4] Thomas G. Graeber,[3,5] John Wongvipat,[1,4,5] M. Luisa Iruela-Arispe,[6] JianFeng Zhang,[7,8] Robert Matusik,[7] George V. Thomas,[2,*] and Charles L. Sawyers[1,4,5,*]

[1]Departments of Medicine, Urology, Molecular and Medical Pharmacology
[2]Department of Pathology
[3]UCLA-DOE Institute for Genomics and Proteomics
[4]Jonsson Comprehensive Cancer Center; David Geffen School of Medicine, University of California, Los Angeles, California 90095
[5]Howard Hughes Medical Institute
[6]Department of Molecular, Cell and Developmental Biology, University of California, Los Angeles, California 90095
[7]Department of Urology, Vanderbilt University School of Medicine, Nashville, Tennessee 37232
[8]Department of Dermatology, University of Alabama, Birmingham, Alabama 35294
*Correspondence: gvthomas@mednet.ucla.edu (G.V.T.); csawyers@mednet.ucla.edu (C.L.S.)

Summary

Increased *Myc* gene copy number is observed in human prostate cancer. To define Myc's functional role, we generated transgenic mice expressing human *c-Myc* in the mouse prostate. All mice developed murine prostatic intraepithelial neoplasia followed by invasive adenocarcinoma. Microarray-based expression profiling identified a *Myc* prostate cancer expression signature, which included the putative human tumor suppressor *NXK3.1*. Human prostate tumor databases revealed modules of human genes that varied in concert with the *Myc* prostate cancer signature. This module includes the Pim-1 kinase, a gene known to cooperate with Myc in tumorigenesis, and defines a subset of human, "*Myc*-like" human cancers. This approach illustrates how genomic technologies can be applied to mouse cancer models to guide evaluation of human tumor databases.

Introduction

The mouse has long been exploited as a model to study the molecular basis of human cancers and test novel therapies. Recent advances in mouse engineering techniques and in genomics tools to query mouse tumor tissue allow a more global comparison of these models to human cancer. We have addressed this issue in a novel transgenic model of mouse prostate cancer using the human *Myc* gene as the initiating event. *Myc* has been widely implicated in many human cancers (Nesbit et al., 1999) and is sufficient to give cancer phenotypes in various murine tissues when expressed as a transgene (Jensen et al., 2002; Moroy et al., 1991; Nesbit et al., 1999; Pelengaris et al., 1999, 2002a, 2002b; Zhang et al., 2000b). We focused our studies on the role of Myc in prostate cancer for two reasons. First, several independent, publicly available gene expression profiling datasets of human prostate tumors (Dhanasekaran et al., 2001; Singh et al., 2002; Welsh et al., 2001) are available for comparison to mouse models. Second, the functional role of Myc in human prostate cancer remains undefined. Numerous studies of human prostate cancer have demonstrated increased *Myc* gene copy number in up to 30% of tumors, even at the preneoplastic stage called prostate intraepithelial neoplasia (PIN) (Jenkins et al., 1997; Nesbit et al., 1999; Qian et al., 1997; Sato et al., 1999), but this finding is not conclusive because *Myc* is one of many genes localized to this 8q24 amplicon (Elo and Visakorpi, 2001).

Efforts to define the mechanism by which Myc induces cancer have identified a number of effects such as increased cell proliferation, which clearly contribute to tumorigenesis. Among the most perplexing has been the well-documented proapoptotic activity of Myc, particularly when serum or other survival factors are limiting (Ahmed et al., 1997; Evan et al., 1992; Pelengaris et al., 2002b; Prendergast, 1999). Recent transgenic models have clarified how the seemingly paradoxical death-promoting activity of Myc can lead to cancer. Expression of a hormone-regulated *Myc* transgene in the skin rapidly induces epidermal hyperplasia and papillomas, with associated increases in cellu-

SIGNIFICANCE

Previous attempts to model human prostate cancer by manipulating expression of genes implicated in human tumors have fallen short, in that most fail to give invasive carcinomas. Here we demonstrate that mice expressing human *Myc* in the prostate reliably develop murine prostatic intraepithelial neoplasia, then invasive adenocarcinomas. These tumors share molecular features with human prostate cancer, as defined by array-based expression profiling, such as loss of the candidate human prostate tumor suppressor gene *Nkx3.1* and upregulation of the serine/threonine kinase *Pim-1*. This model provides a novel tool for identification and functional evaluation of genetic events in prostate cancer progression and for preclinical therapeutic studies.

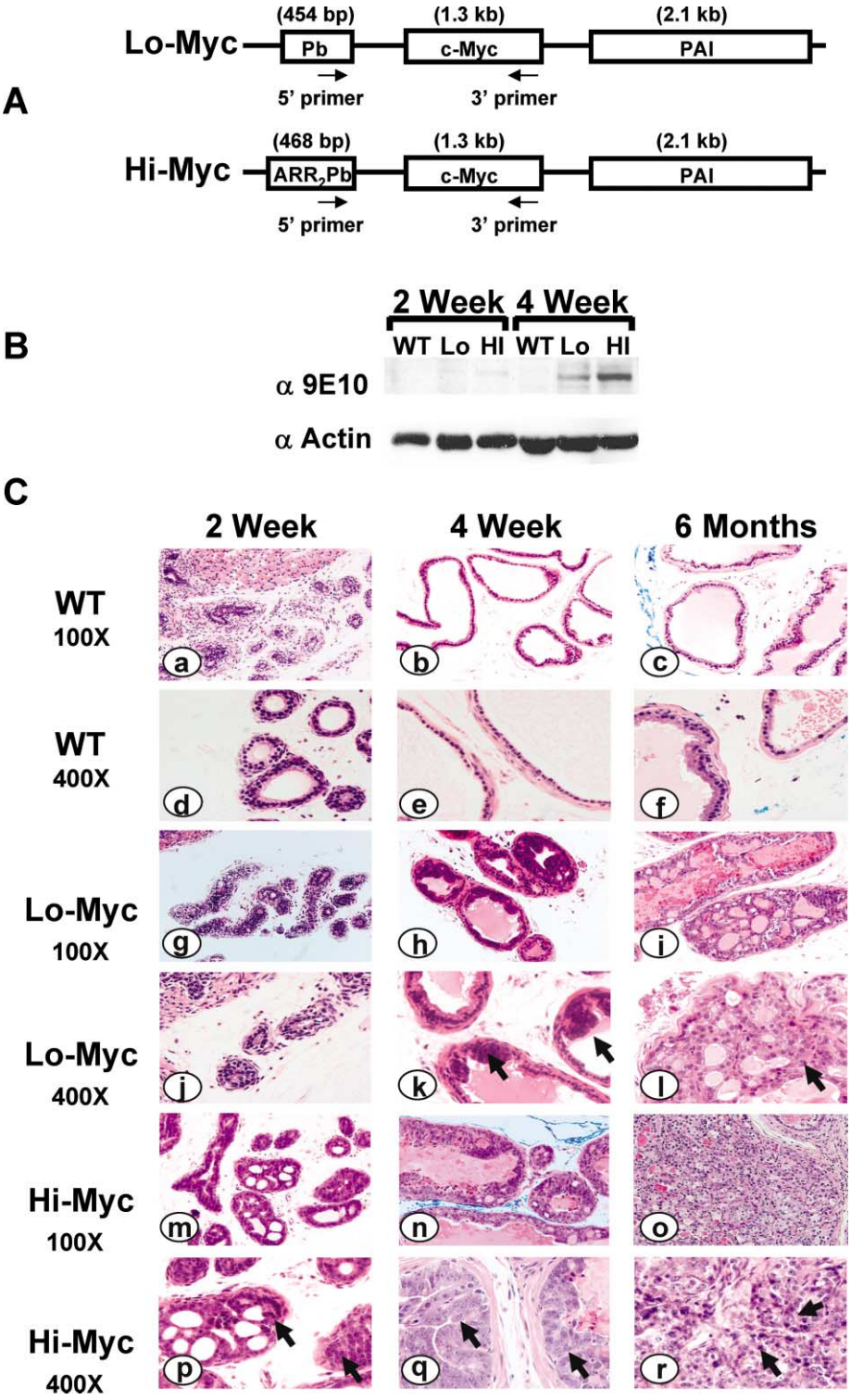

Figure 1. Generation and characterization of *Myc* transgenic mice

A: Construction of the Lo-Myc and Hi-Myc transgene. cDNA encoding human *c-Myc* was cloned along with the insulin polyA site downstream of either the rat probasin or the modified small composite probasin promoters. Primers specific to each promoter and human Myc were used to confirm germline transmission of the transgene.

B: Comparative expression of Myc in the mouse prostate. Total protein was isolated from 2- and 4-week-old wild-type, Hi-Myc and Lo-Myc mice. Myc expression was determined by Western blot using the human-specific α-9E10 Myc antibody. Transgene expression is seen as early as 2 weeks in both transgenic mice, and expression increases as mice reach puberty by 4 weeks. β-actin was used as a loading control.

C: Kinetics of mPIN and cancer progression in Hi-Myc and Lo-Myc transgenic mice. Low (100×) and high (400×) magnification views of the dorsolateral prostate are shown. Hi-Myc mice exhibit mPIN as early as 2 weeks (m and p) compared to 4 weeks (h and k) in the Lo-Myc transgenic animals. Hi-Myc mice go on to develop invasive prostatic adenocarcinoma by 6 months (o and r) whereas the Lo-Myc animals continue to exhibit mPIN at the same time point (i and l). Arrows indicate nuclear atypia.

lar proliferation and minimal evidence of apoptosis (Pelengaris et al., 1999, 2002a). However, these tumors rapidly apoptose when cultured ex vivo, presumably due to the lack of critical survival factors present in the mouse dermis. In contrast, transgenic expression of *Myc* in the pancreas causes rapid involution of insulin-producing islet cells, due to increased apoptosis, and subsequent onset of diabetes (Pelengaris et al., 2002a, 2002b). When complemented with a *Bcl*X_L transgene, the mice no longer display the apoptotic phenotype, but develop aggressive islet cell cancers. These experiments demonstrate that the response to *Myc*

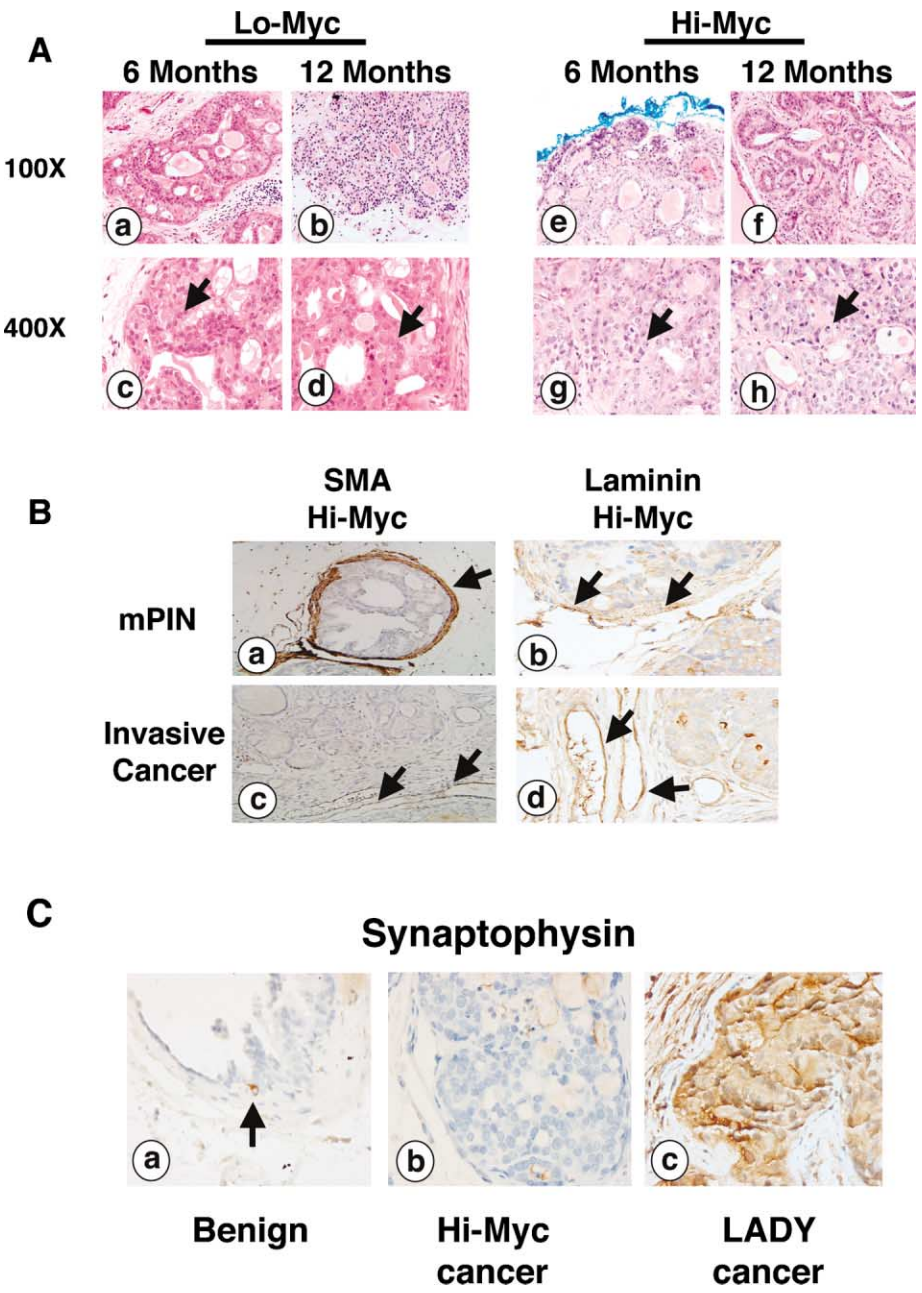

Figure 2. Development of cancer in Hi-Myc and Lo-Myc transgenic animals without neuroendocrine differentiation

A: Longer latency for cancer progression in Lo-Myc mice. Dorsolateral lobes from 6 and 12 month transgenic mice reveal invasive adenocarcinoma at 12 months in the Lo-Myc animals (a–d). In contrast, invasive tumor is already apparent by 6 months (e and g) in the Hi-Myc mice. Arrows depict nuclear atypia associated with mPIN and cancer.

B: Presence of an intact fibromuscular layer and basement membrane, as shown by the positive SMA and laminin immunostaining (arrows, a and b), confirms the in situ nature of the mPIN lesions. In contrast, SMA and laminin staining are absent in the invasive tumors (c and d). Contractile smooth muscle surrounding blood vessels serve as internal positive controls (arrows, c and d).

C: Tumors do not undergo neuroendocrine differentiation. Synaptophysin immunostaining identifies the rare neuroendocrine cell normally present in murine prostates (a, arrow). The Hi-Myc prostate with invasive adenocarcinoma shows no synaptophysin staining (b) whereas the dorsolateral lobes of the LADY mice stain positive (c). Images depict the dorsolateral lobes.

expression in different tissues is critically dependent on associated survival signals and suggest a role for secondary cooperating events in rescuing cells from *Myc*-induced apoptosis.

To determine the consequence of increased *c-Myc* expression in the prostate, we generated transgenic mice expressing human *c-Myc* from two different strength prostate-specific promoters. In all founder lines, Myc expression resulted in complete penetrance of mouse prostatic intraepithelial neoplasia (mPIN), which progressed to invasive adenocarcinoma within 6 to 12 months of age. mPIN lesions were observed as early as 2 to 4 weeks, providing evidence that Myc is sufficient to induce a preneoplastic phenotype in the prostate. These cells demonstrated a high rate of proliferation that overcame the apoptotic effect of Myc expression, suggesting that prostate tissue contains survival factors that allow the cells to tolerate increased Myc protein. Microarray expression profiling studies defined a *Myc* prostate cancer expression signature that shares features with human prostate cancer and implicates candidate genes in tumor progression. For example, expression of the putative human prostate tumor suppressor gene *NXK3.1* (Bowen et al., 2000; He et al., 1997; Voeller et al., 1997) was detected in Myc-induced mPIN lesions but absent in invasive cancers. Furthermore, analysis of human cancer databases with the murine *Myc*

Table 1. High penetrance of mPIN and cancer in *Myc* transgenic mice

A. Penetrance in Myc transgenic mice

Strain	Age	# Mice	Phenotype	Comments
Hi-Myc	≤3 months	16	16/16 mPIN	mPIN in 4/4 mice at 2 weeks
	≥6 months	20	19/20 invasive cancer 1/20 mPIN*	
Lo-Myc	≤10 months	10	8/10 mPIN*	2 mice at 2 weeks were benign
	≥10 months	10	10/10 invasive cancer	

B. Timing of mPIN and cancer progression in Myc transgenic mice

	mPIN	mPIN/cancer transition	Invasive cancer
Hi-Myc	2 weeks	3 to 6 months	>6 months
Lo-Myc	4 weeks	6 to 12 months	>12 months

Mice were aged to the appropriate time point and sacrificed for histological analysis. Age, phenotype, and number of mice are listed for both the Hi-Myc and Lo-Myc transgenic models. Generally, in the Hi-Myc model, all mice ≤3 months developed mPIN and all animals older than 6 months developed cancer. In the Lo-Myc model, most animals less than 12 months developed mPIN and cancer after 1 year. Only a few exceptions (*) are observed.

gene signature uncovered gene clusters whose expression was tightly correlated in human prostate, breast, and ovarian cancer. The murine *Myc* prostate tumor signature genes that are most consistently coexpressed in the human cancers included *Pim-1*, previously shown to cooperate with Myc in mouse tumor models. Collectively, these findings define a novel transgenic mouse model of prostate cancer and demonstrate the utility of comparing mouse and human cancer expression databases.

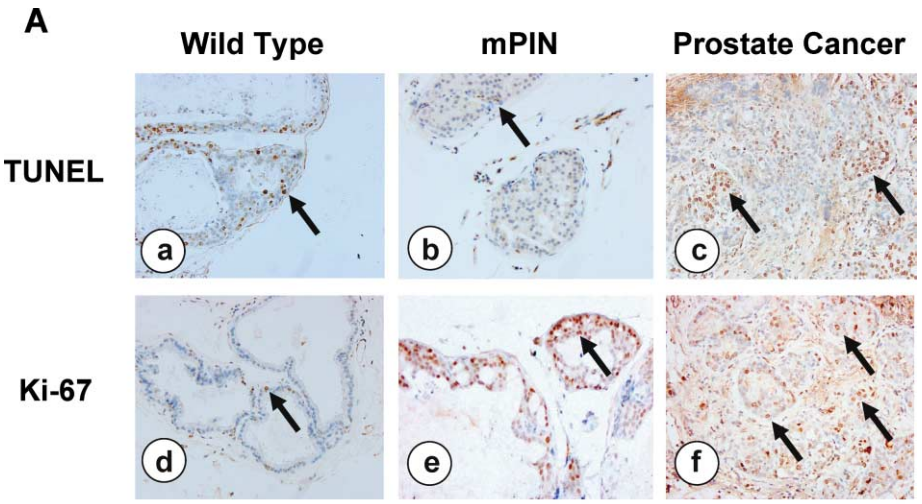

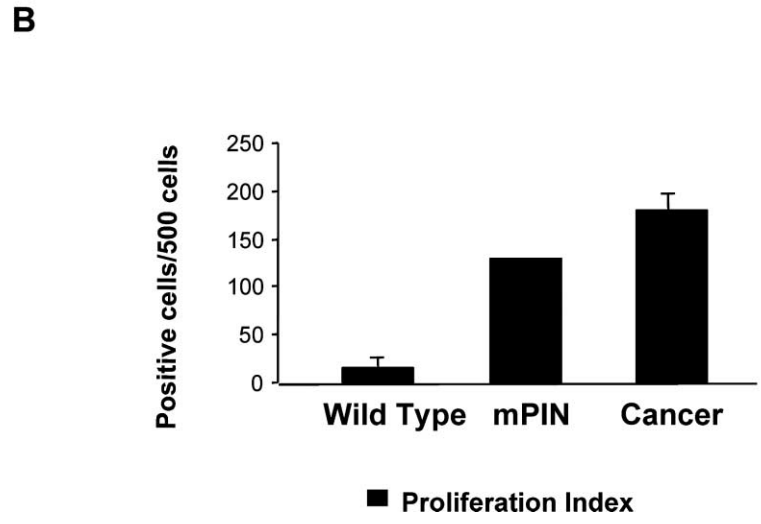

Figure 3. Myc expression gives a proliferative advantage to prostate tissue

A: Ki67 and TUNEL labeling revealed an increase in both proliferation and apoptosis as cells progress from wild-type (a and d) to mPIN (b and e) and finally to invasive cancer (c and f). Images of the dorsolateral lobes are shown.

B: Proliferation increases as mice develop prostate cancer. A total of 500 cells were counted from five high-power fields and the number of Ki67-positive cells (proliferative index) was scored and graphed.

Results

Transgenic expression of Myc in the prostate induces mPIN, then invasive adenocarcinoma with reproducible kinetics and high penetrance

Two different prostate-specific transgenic expression constructs (probasin-*Myc* and ARR_2/probasin-*Myc*) were used to vary the dosage of Myc expression specifically in the prostate (Figure 1A). Expression from the probasin promoter begins at a low level in the prostate at 1 to 2 weeks of age and increases with rising levels of androgen as the mice reach puberty between 4 and 8 weeks (Figure 1B). The ARR_2/probasin promoter contains two additional androgen response elements, which boost the level of androgen-dependent expression (Figure 1B) (Wu et al., 2001; Zhang et al., 2000a). Multiple founders were obtained for each construct (seven from the ARR_2/probasin-*Myc* and three from the probasin-*Myc*), prostate-specific Myc protein expression was confirmed, and independent lines from each construct were expanded for phenotypic analysis. Based on the levels of transgene expression, the probasin-*Myc* mice and ARR_2/probasin-*Myc* mice were designated Lo-Myc and Hi-Myc, respectively.

Mouse PIN (mPIN) is characterized histologically by the presence of multifocal proliferative lesions of atypical epithelial cells affecting several existing ductules within individual lobes. mPIN usually displays distinctive architectural growth patterns, e.g., cribiform and/or tufting, but these cells must also exhibit progressive nuclear atypia. Atypical cells are characterized by the presence of large irregular nuclei, exhibiting hyperchromatic or vesicular chromatin patterns, with prominent nucleoli and amphophilic cytoplasm. In both the Lo-Myc and Hi-Myc mice, multifocal proliferative lesions affecting several ductules within the individual lobes were observed in the dorsolateral (Figures 1Ck, 1Cl, 1Cp, and 1Cq) and ventral lobes and to a lesser extent in the anterior lobe. Cribiform and tufting growth patterns of the secretory epithelial layer were also observed (Figures 1Ck, 1Cl, 1Cp, and 1Cq) as well as progressive nuclear atypia (Figure 1C, arrows), distinguishing these lesions from benign hyperplasia. Finally, the in situ nature of these lesions was confirmed by the presence of an intact basement membrane and fibromuscular layer, as demonstrated by positive laminin and smooth muscle actin (SMA) immunohistochemical staining, respectively (Figures 2Ba and 2Bb).

The mPIN lesions in both Lo-Myc and Hi-Myc mice subsequently progressed to invasive adenocarcinomas, as seen by the extension of numerous nests of acini consisting of cytologically atypical cells into the prostatic stroma and periprostatic adipose tissue. These acini exhibit crowding, irregular contours and haphazard growth patterns (Figures 1Co and 2Ab, 2Ae, and 2Af). The mPIN/cancer transition was evident by 3 to 6 months in all lobes of the Hi-Myc mice and by 10 to 12 months in the Lo-Myc mice, suggesting that the dosage of Myc may affect the rate of disease progression (Figure 2A). Invasion was confirmed by the absence of laminin and SMA staining, which documents penetration through the basement membrane and the fibromuscular layer, respectively (Figures 2Bc and 2Bd). Foci suggestive of lymphovascular invasion were also noted in some cancers (data not shown). mPIN was always found in glands adjacent to the invasive tumor. The penetrance of mPIN and cancer was essentially 100 percent in all founder lines with reliable kinetics (Table 1), indicating the potential utility of this model for studying progression from mPIN to cancer and for preclinical therapeutic studies.

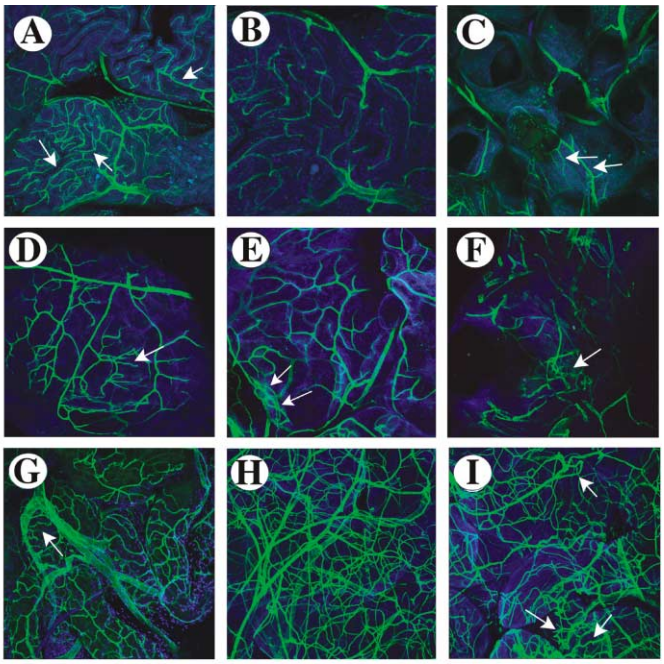

J **Vascular density (mm)²**

	2 mo.	1 year
Wildtype animals	23 (±3)	21 (±6)
Transgenic animals	34 (±5)	45 (±9)

Figure 4. Vascular profile of myc tumors

Mice were injected with FITC-conjugated *Lycopersicum esculentum* lectin that binds to the luminal surface of blood vessels (in green). Topo 3 was also used for visualization of nuclei (in blue). **A–C:** Wild-type animals (**A**, 2 month; **B** and **C**, 1 year). Note that the blood vessels travel in the stroma justaposed to the prostate epithelium. There is no increase in vascular density in the prostate of 2-month-old versus 1-year-old wild-type mice; **D–F:** Transgenic animals (2 months). Increased vascular density and tortuosity in vessels is associated with early transformation stages; **G–I:** In transgenic animals (1 year), higher degrees of vascular density and disorganization characterize late-stage tumors. Each panel represents a different animal. In each case, the anterior lobe was photographed. **J:** Table showing the vascular density (mm^2) in Hi-Myc and control littermates.

To date, the only known murine models of prostate cancer that progress beyond the mPIN stage are the SV40 large T antigen models of prostate cancer (TRAMP, C3-Tag, and LADY) (Garabedian et al., 1998; Greenberg et al., 1995; Kasper et al., 1998; Masumori et al., 2001; Shibata et al., 1996). One potential shortcoming of the T antigen models is the high frequency of neuroendocrine differentiation that occurs, as recognized by its typical histologic features and subsequent confirmation by

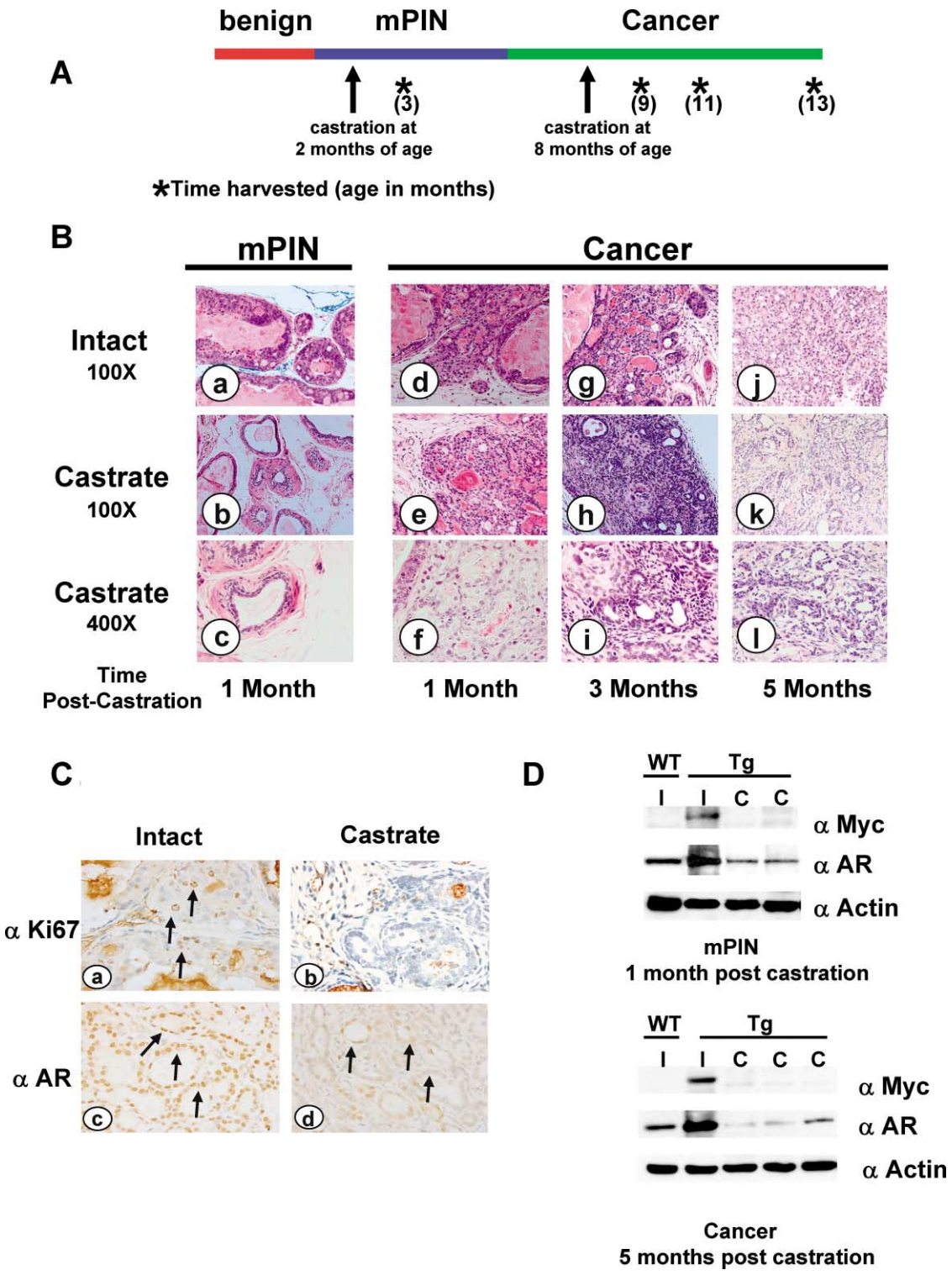

Figure 5. Effects of castration on Myc-induced mPIN and prostate cancer

A: Schematic of castration experiment using the Hi-Myc transgenic mice. Mice were either castrated at 2 months of age with mPIN (n = 3) or castrated at 8 months after tumors had developed (n = 9) and then sacrificed 1, 3, or 5 months post-surgery (*). Prostate lobes were microdissected and analyzed by H&E.

B: Castration causes the reversion of mPIN lesions 1 month post-surgery (a–c). Castration at later time points results in partial regression of the primary tumors, when examined at 1 (d–f), 3 (g–i), and 5 (j–l) months post-surgery. In each panel, images depict H&E stains of the dorsolateral lobes of the prostate.

C: Residual, nonproliferating tumor remains following castration. Immunohistochemistry using α-Ki67 shows a decrease in the number of Ki67-positive cells following castration (compare a and b). Immunohistochemistry using the α-androgen receptor (AR) antibody also shows a decrease in the number of AR-positive cells as well as an increase in cytoplasmic staining post-surgery (compare c and d). Images represent the dorsolateral lobes.

immunohistochemical stains such as synaptophysin or chromogrannin A (Figure 2Cc) (Masumori et al., 2001). Although human prostate cancers can occasionally possess a completely neuroendocrine phenotype (e.g., small cell carcinoma), the majority do not. The mPIN and invasive carcinoma lesions detected in the Lo-Myc and Hi-Myc mice do not exhibit the morphologic features of neuroendocrine carcinomas, and this is further confirmed by the lack of immunostaining with synaptophysin (Figure 2C, compare b and c). Therefore, the Lo- and Hi-Myc mice represent novel models for human prostatic adenocarcinoma that may offer advantages over current models.

Myc expression in the mouse prostate induces proliferation, apoptosis, and angiogenesis

Myc can induce proliferation, apoptosis, and angiogenesis in many cell types (Amati et al., 1998; Dang, 1999; Pelengaris et al., 2002a, 2002b; Prendergast, 1999; Watnick et al., 2003). To understand the cellular effects of Myc overexpression in the prostate, we first tested for proliferation using Ki67 immunohistochemistry and apoptosis using TUNEL assays. Immunohistochemistry showed an increase in Ki67 staining in both mPIN and tumor lesions when compared to wild-type samples, as shown in Figure 3A (d–f). Ki67 staining was quantified by counting a total of 500 cells. The proliferative index increased from 20 in wild-type cells to 140 in mPIN lesions and 180 in tumor tissue (Figure 3B). TUNEL assays performed on the same tumor showed that Myc was also capable of inducing apoptosis in the mouse prostate (Figures 3Aa–3Ac). These results demonstrate that Myc induces both proliferation and apoptosis in the mouse prostate; however, the rapid development of mPIN suggests that, like epidermal cells (Pelengaris et al., 1999), the prostate may contain survival signals that rescue much of the gland from Myc-induced apoptosis.

Myc can also induce angiogenesis in certain tissues, a property that likely contributes to tumor progression and metastasis (Elenbaas et al., 2001; Hurlin et al., 1995; Pelengaris et al., 1999; Watnick et al., 2003). Therefore, we characterized changes in vascular density in the Hi-Myc tumor model at the mPIN and invasive cancer stages, using wild-type and transgenic animals at 2 and 12 months of age (Figures 4A–4I). Blood vessels were identified in green after perfusion with FITC-conjugated *Lycopersicum esculentum* lectin as previously described (Rodriguez-Manzaneque et al., 2001). Increased vascular density was detected as early as 2 months in transgenic animals with mPIN (Figures 4D–4F and 4J), and vascular density doubled with progression to invasive adenocarcinoma at the 12 month time point (Figures 4G–4I and 4J). Vascular alterations, such as tortuosity and disorganization of vessels common to tumors, were noted at 2 months and became significantly pronounced by 12 months.

Effects of hormone ablation on the initiation and maintenance of Myc-induced prostate lesions

Since hormone ablation therapy is the primary clinical treatment for prostate cancer patients with advanced stage disease, we examined the effect of castration on disease progression in the Hi-Myc transgenic mice. Since the ARR_2PB promoter is regulated by androgen, interpretation of the effect of hormone ablation must consider potential effects on expression of the transgene. Mice were either castrated at 2 months when they had definite mPIN lesions ($n = 3$) or at 8 months ($n = 9$) after tumors had developed, then analyzed either 1, 3, or 5 months post-castration (Figure 5A). All mice castrated at 2 months of age have complete regression of mPIN within one month of castration (Figures 5Ba–5Bc). This was correlated with absence of detectable transgene expression by immunoblot (Figure 5D). This result indicates that Myc-induced mPIN is reversible, similar to other Myc-induced neoplastic phenotypes in tetracycline-regulated models (Jain et al., 2002; Karlsson et al., 2003). Similarly, all mice with prostate cancer (castrated at 8 months of age) had histologic evidence of regression and fibrosis at all time points post-castration (Figures 5Bd–5Bl). However, unlike mPIN lesions (Figures 5Ba–5Bc), all these mice had residual tumor present even 5 months post-castration (Figures 5Bk and 5Bl). The residual tumors were apparently quiescent since we were unable to document proliferation of tumor cells by nuclear Ki67 staining (Figures 5Ca and 5Cb). Immunoblot studies showed loss of Myc expression in the residual tumors, indicating silencing of the transgene. Also, these tumors expressed lower levels of AR protein, a known consequence of castration (Figure 5D). Following castration, we also observed weak heterogenous expression of AR with predominately cytoplasmic localization, compared to nuclear localization in the intact mice (Figure 5C, compare c and d). Collectively, these findings establish that AR is inactive and the *Myc* transgene is not expressed in these residual, post-castration tumors. The fact that these tumors fail to fully regress, unlike the mPIN lesions, suggests that additional genetic events may have occurred that maintain tumor cell survival. Larger cohorts of mice will be followed for longer time intervals to determine if these mice eventually relapse with progressive, hormone refractory prostate cancer.

An expression signature for Myc-driven murine prostate cancer

The high penetrance and reliable kinetics of the PIN/cancer transition in these Myc models provides an experimental opportunity to define the cooperating molecular events involved in Myc-driven prostate cancer progression. We isolated dorsal, lateral, ventral, and anterior prostate lobes from Hi-Myc transgenic mice and nontransgenic littermate controls at various time points during the mPIN/cancer transition for gene expression profiling experiments. Samples were divided for parallel analysis by mouse Affymetrix arrays for gene expression and comparative genome hybridization arrays (array CGH) for chromosomal gains and losses. Matched tissue was saved for histological and immunohistochemical studies. The expression signatures for wild-type and transgenic (mPIN and cancer combined) were strong enough to be recognized by unsupervised clustering with only one error (Figure 6A). Parallel array CGH experiments were also conducted using genomic DNA from these samples to look for evidence of chromosomal gains or losses that might accompany these expression changes. To date, we have not

D: Myc transgene expression is turned off and AR levels decrease following castration. Immunoblots of prostate lysates isolated from wild-type or transgenic intact (I) or castrate (C) mice were performed using the α-Myc (9E10) and α-AR antibodies. All mice showed a loss of Myc expression following castration as well as a decrease in AR levels. Actin serves as a loading control.

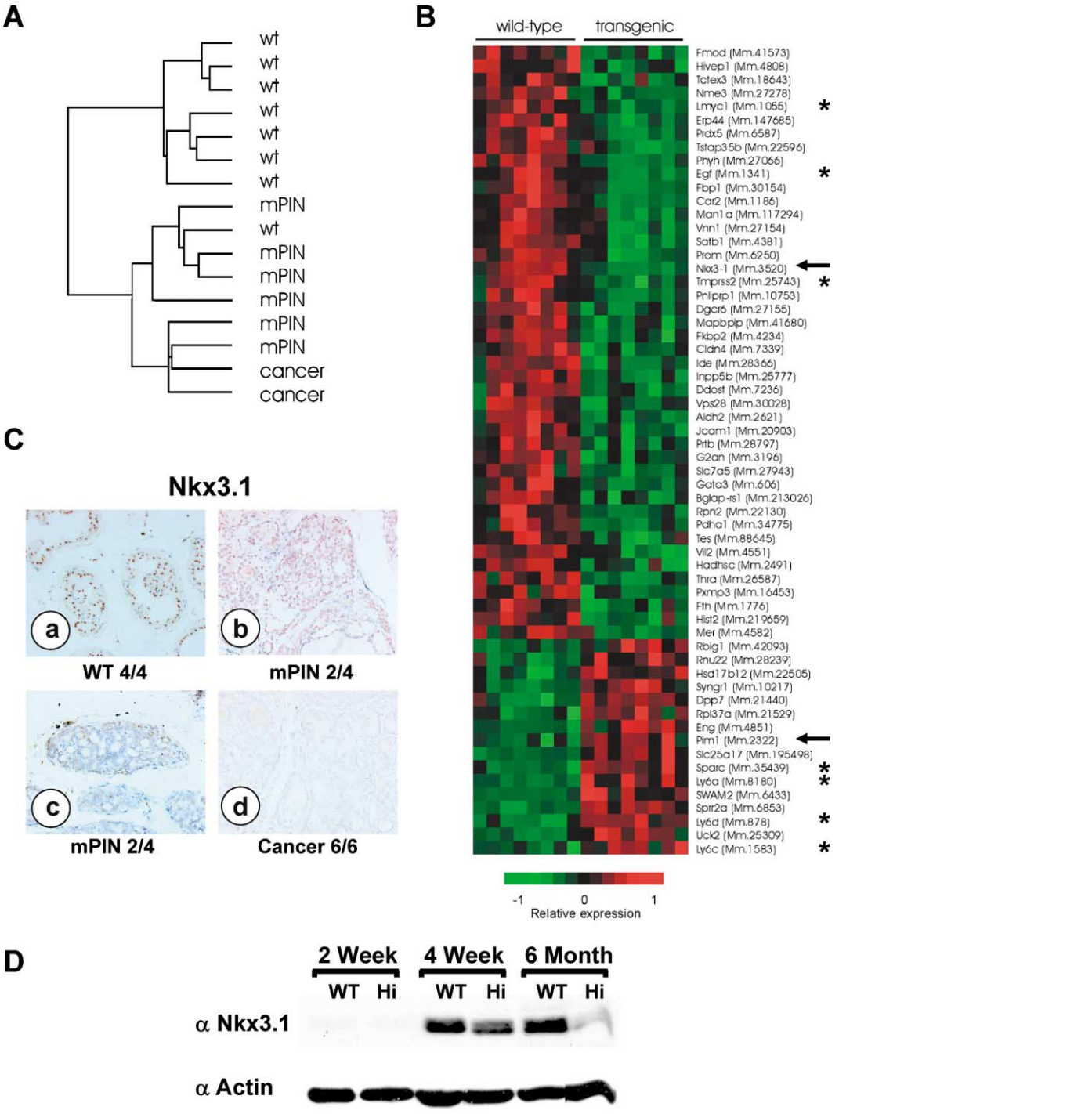

Figure 6. Microarray analysis identifies a distinct expression signature of genes in *Myc* transgenic animals

A: Unsupervised clustering classifies samples as either wild-type (wt) or transgenic (mPIN and cancer) with one exception. The raw gene expression data is available at http://doe-mbi.ucla.edu/myc_driven_prostate_cancer/.

B: Genes differentially expressed between wild-type and transgenic mice. The top 60 non-EST genes are included, and a full list is available in the Supplemental Data on the *Cancer Cell* website. The list includes two genes known to be involved in human prostate cancer, *Nkx3.1* and *Pim-1* (arrows). Nkx3.1 expression is lost in transgenic samples and Pim-1 is upregulated consistent with published human data (Bowen et al., 2000; Dhanasekaran et al., 2001). Expression values of each gene are normalized to have a mean of zero and standard deviation of one across the samples.

C and **D:** Nkx3.1 protein levels diminish in mPIN lesions and are lost in tumors samples consistent with microarray data. Immunohistochemistry shows a variable level of Nkx3.1 in mPIN lesions that is completely absent in tumors (**C**, compare panels b and c to d). Western blot analysis using the Nkx3.1 antibody shows a consistent loss of Nkx3.1 expression as tumors progress from mPIN lesions (**D**). The dorsolateral lobes are depicted in each image.

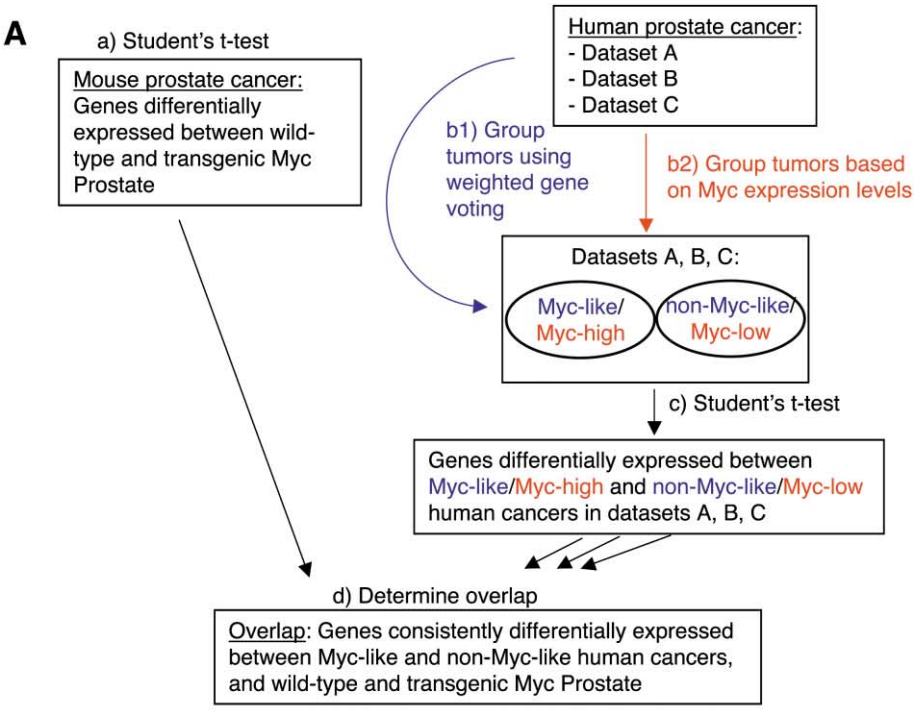

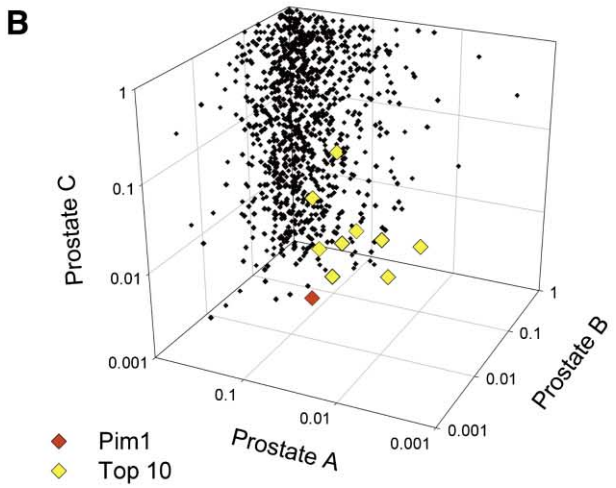

Figure 7. Cross-species expression module comparison algorithm

A: Schematic of the computational algorithms used to identify genes consistently regulated in *Myc* transgenic and human prostate cancers based on predicted *Myc* status (blue path) or Myc expression levels (red path) (see Experimental Procedures).

B: Scatter plot showing the genes differentially expressed between *Myc*-like and non-*Myc*-like human tumors in multiple datasets. In the graph, each point represents a gene found in the Prostate A-C (Dhanasekaran et al., 2001; Singh et al., 2002; Welsh et al., 2001) human cancer datasets. For each gene, the Student t test p values reflecting the degree of differential gene expression between *Myc*-like and non-*Myc*-like human tumors were determined and plotted (see schematic, panel A). The top 10 entries from Table 2A are indicated by yellow and red (Pim-1) diamonds.

observed any genomic changes in mPIN lesions or cancers, but it is important to note that current mouse BAC arrays are limited to 3 Mb resolution and we cannot rule out smaller gains or losses (data not shown).

Next we generated a supervised gene list that distinguishes wild-type mice from *Myc* transgenic mice. We ranked genes by the degree of differential expression between wild-type and transgenic mice using the Student's t test. The 60 most differentially expressed genes, excluding ESTs, are shown in Figure 6B, and the complete list is available as Supplemental Data at http://www.cancercell.org/cgi/content/full/4/3/223/DC1. The genes on this list can potentially come from several categories, including genes modulated generally in tumorigenesis (e.g., from expansion of a particular cell type) or specifically in prostate tumorigenesis or Myc-driven tumorigenesis (Coller et al., 2000). Additionally, the transgenic *Myc* gene list can include Myc transcriptional targets or genes whose up- or downregulation complements Myc expression during tumorigenesis. Since the *Myc* transgene is expressed as early as 1 to 2 weeks of age, the transgenic *Myc* gene list can include genes directly or indirectly regulated by *Myc* transcription. In an attempt to address this issue, we compared our list of Myc-driven tumor-associated gene changes to various lists of *Myc* target genes and found that some genes and gene families are in common, but we were unable to demonstrate any statistically significant overlap. Thus, not unexpectedly, our list does not appear to be dominated by direct Myc transcriptional targets. A better distinction between *Myc* primary and secondary target genes and genes more generally associated with prostate cancer will be possible by future comparison of the Myc-driven tumors to other mouse prostate

cancer models (Wu et al., 2003 [this issue of *Cancer Cell*]). The substantial role of Myc in cellular proliferation (Gartel and Shchors, 2003; Sears and Nevins, 2002) raises the possibility that the Myc prostate expression signature is strongly comprised of genes associated with proliferation. However, a comparison of the Myc prostate signature with several previously published proliferation signatures did not show statistically significant overlap (Lam et al., 2001; Perou et al., 1999; Rosenwald et al., 2003; Whitfield et al., 2002).

Several genes of interest appeared on the list and include *L-Myc*, normally expressed at high levels in differentiated prostate tissue (Luo et al., 2001), *Tmprss2*, a serine protease overexpressed in a majority of prostate cancer patients (Vaarala et al., 2001), *Sparc*, an antiadhesive protein that is differentially expressed during human prostate cancer progression (Thomas et al., 2000), *EGF*, which has been implicated in prostate cancer progression (Kim et al., 2003), and several *Ly6* genes that belong to the same family as prostate stem cell antigen (*PSCA*), a cell surface antigen overexpressed in human prostate cancer (Jalkut and Reiter, 2002) (Figure 6B, asterisks). We focused our attention on two genes, *Nkx3.1* and *Pim-1*, for the reasons discussed below (Figure 6B, arrows).

Loss of Nkx3.1 protein expression marks the transition from mPIN to invasive cancer

The microarray finding of reduced levels of *Nkx3.1* mRNA in transgenic mice is of particular interest because human *Nkx3.1* is a putative tumor suppressor gene in human prostate cancer (He et al., 1997). Loss of heterozygosity at the *Nkx3.1* locus occurs commonly in human prostate tumors due to large deletions at 8p22, but it has proved difficult to directly implicate *NXK3.1* as the relevant gene since mutations do not occur in the remaining allele (Voeller et al., 1997). To distinguish between the possibilities that *Nkx3.1* may be a Myc target gene (since decreased *Nkx3.1* mRNA levels were found in transgenic mice with mPIN and cancer as compared to wild-type controls) versus a complementary secondary event, we examined Nkx3.1 protein expression in situ using immunohistochemical studies. Nkx3.1 protein expression was consistently present in mPIN lesions at variable levels (Figures 6Cb and 6Cc), but was undetectable in all the cancers isolated from both the Hi-Myc and Lo-Myc strains (Figure 6Cd). Immunoblot studies of prostate lysates from tumor-bearing mice also showed a marked decrease in Nkx3.1 protein expression when compared to lysates from wild-type or mPIN mice (Figure 6D). These results indicate that Nkx3.1 loss is distinct from the onset of Myc expression and raise the possibility that Myc gain and Nkx3.1 loss may be critical cooperating events in the mPIN/prostate cancer transition.

Cross-species bioinformatic comparison of mouse and human datasets implicates Pim-1 in Myc-associated cancer progression

The large number of genes in the Myc prostate signature emphasizes the need for strategies to prioritize genes for functional evaluation. Accordingly, we used two related methods to search for gene expression patterns common to both our Myc transgene model and human prostate cancer. A schematic of our "cross-species expression module comparison" approaches is shown in Figure 7A.

In the first method, we predicted the *Myc* status of the human tumors using the genes from the Myc mouse prostate signature (Figure 6B) in a gene expression-based class prediction analysis (Golub et al., 1999), and then identified the genes most consistently differentially expressed between *Myc*-like and non-*Myc*-like human tumors and between wild-type and *Myc* transgenic mouse prostates (Figure 7A, blue path) as follows: (a) We began with our list of genes differentially expressed between wild-type and *Myc* transgenic mice. We then identified the human orthologs for these genes using the HomoloGene database (http://www.ncbi.nlm.nih.gov/HomoloGene/) and determined which were present in three human prostate cancer gene expression datasets. (b1) We ascertained whether the human tumors were more *Myc*-like or non-*Myc*-like using a weighted gene voting prediction algorithm (Golub et al., 1999) and then (c) made ranked lists of the genes most differentially expressed between the human tumors in these two categories using the Student's t test. Finally, (d) we identified the genes most consistently differentially expressed between *Myc*-like and non-*Myc*-like human tumors based on the overlap between the ranked lists from the mouse and the three human datasets. In summary, this method investigates whether the coexpressed mouse *Myc* prostate signature genes are also coexpressed in human cancers and identifies the most consistently regulated genes in the *Myc* prostate tumor expression module.

We first performed this analysis using three publicly available prostate cancer datasets (Dhanasekaran et al., 2001; Singh et al., 2002; Welsh et al., 2001). The most striking result was the presence of *Pim-1* at the top of our list (Table 2A, Figure 7B). *Pim-1* was on our original list of genes differentially expressed between wild-type and Myc transgenic prostates with a rank of 113 (Figure 6B; Supplemental Data on *Cancer Cell* website). The reprioritization of Pim-1 to a rank of 1 is noteworthy, in that Pim-1 has previously been shown to cooperate with Myc in lymphomagenesis (van Lohuizen et al., 1989, 1991), and suggests that this approach could be used with other transgenic cancer models and human datasets to identify complementing oncogenes.

To investigate whether the Myc expression signature identified using our transgenic mice is prostate specific, we added breast and ovarian cancer datasets to our cross-species comparison algorithm. We again found that one of the most consistently regulated genes in the Myc expression module is *Pim-1* (data not shown). This result is consistent with the fact that Myc expression is implicated in the progression of many tumor types (Nesbit et al., 1999).

In the second method, we inferred the Myc status of the human tumors based on whether their Myc expression level was above or below the mean Myc expression level for the dataset (step b2) and then followed the rest of the procedure outlined above (Figure 7A, *red path*). This procedure resulted in slightly different groupings of the human samples and accordingly a slightly different list of consistently modulated genes (Table 2B). It remains to be determined from independent data (e.g., *Myc* gene amplification status of human tumors) whether the predicted Myc status from the *Myc* mouse prostate tumor signature or the inferred Myc status from the Myc expression levels better reflects the true Myc status of human tumors. However, both methods result in *Pim-1* and *GNAS1* (G protein, α stimulating activity polypeptide 1) in the top 10 of the list of consistently modulated genes. Additionally, this second method revealed two other genes previously implicated in either prostate

Table 2. Myc prostate cancer signature genes consistently regulated in *Myc* transgenic and human prostate cancers

A: Myc signature genes consistently regulated in *Myc* transgenic and human prostate cancers based on predicted Myc status (method b1)[a]

	p values									
		Datasets								
Rank[b]	Max	Myc mouse (n = 16)	Human prostate A (n = 14)	Human prostate B (n = 25)	Human prostate C (n = 27)	Direction[c]	UniGene (human)	UniGene (mouse)	Gene abbreviation	Gene description
1	0.05	0.003	0.05	0.01	0.003	up	Hs.81170	Mm.2322	PIM-1	pim-1 oncogene
2	0.09	0.04	0.09	0.09	0.06	down	Hs.108104	Mm.3074	UBE2L3	ubiquitin-conjugating enzyme E2L 3
3	0.09	0.09	0.09	0.07	0.002	up	Hs.77356	Mm.26069	TFRC	transferrin receptor (p90, CD71)
4	0.12	0.12	0.01	0.09	0.01	up	Hs.14601	Mm.4091	HCLS1	hematopoietic cell-specific Lyn substrate 1
5	0.12	0.12	0.04	0.03	0.01	down	Hs.206521	Mm.23335	YME1L1	YME1 (S.cerevisiae)-like 1
6	0.18	0.11	0.04	0.18	0.005	down	Hs.111039	Mm.10265	NMT1	N-myristoyltransferase 1
7	0.18	0.0001	0.03	0.18	0.002	down	Hs.84775	Mm.30251	Hs.84775	Human transposon-like element mRNA
8	0.18	0.01	0.07	0.18	0.01	down	Hs.273385	Mm.197522	GNAS1	G protein, alpha stimulating activity polypeptide 1
9	0.19	0.12	0.19	0.12	0.01	up	Hs.66	Mm.35692	IL1RL1	interleukin 1 receptor-like 1
10	0.20	0.03	0.20	0.18	0.002	down	Hs.26077	Mm.20916	WFS1	Wolfram syndrome 1 (wolframin)
...										
17	0.25	0.25	0.18	0.03	0.01	down	Hs.153863	Mm.27935	MADH6	MAD (mothers against decapentaplegic) homolog 6
18	0.25	0.18	0.09	0.25	0.00	up	Hs.54483	Mm.7491	NMI	N-myc (and STAT) interactor
21	0.25	transgene	0.15	0.25	0.0007	up	Hs.79070	Mm.2444	MYC	v-myc avian myelocytomatosis viral oncogene homolog
38	0.32	0.32	0.08	0.20	0.00	up	Hs.80205	Mm.932	PIM-2	pim-2 oncogene

[a]Human samples were divided into *Myc*-like and non-*Myc*-like groups using a weighted gene voting prediction algorithm trained on the Myc transgenic data using method b1 (Fig 7A, Experimental Procedures).
[b]Genes are ranked by the maximum Student's t test p value across all datasets. Select genes with rank > 10 are shown based on their previous association with Myc.
[c]Up- or downregulated in Myc-high tumors. n, number of samples.

B: Myc signature genes consistently regulated in *Myc* transgenic and human prostate cancers based on Myc expression levels (method b2)[a]

	p values									
		Datasets								
Rank[b]	Max	Myc mouse (n = 16)	Human prostate A (n = 14)	Human prostate B (n = 25)	Human prostate C (n = 27)	Direction[c]	UniGene (human)	UniGene (mouse)	Gene abbreviation	Gene description
1	0.0008	transgene	0.0008	0.0002	6.0E-10	up	Hs.79070	Mm.2444	MYC*	v-myc avian myelocytomatosis viral oncogene homolog
2	0.03	0.01	0.007	0.03	6.9E-05	down	Hs.273385	Mm.197522	GNAS1	G protein, alpha stimulating activity polypeptide 1
3	0.05	0.05	0.004	0.004	0.001	down	Hs.19555	Mm.42855	PTOV1	prostate tumor over expressed gene 1
4	0.06	0.06	0.05	0.03	7.1E-06	up	Hs.40098	Mm.30465	CKTSF1B1	cysteine knot superfamily 1, BMP antagonist 1
5	0.06	0.009	0.06	0.06	0.001	down	Hs.76884	Mm.110	ID3	inhibitor of DNA binding 3, dominant-negative helix-loop-helix protein
6	0.09	0.09	0.09	0.03	0.006	up	Hs.13046	Mm.44552	TXNRD1	thioredoxin reductase 1
7	0.10	0.07	0.10	0.02	0.007	down	Hs.33251	Mm.126873	PPIE	peptidylprolyl isomerase E (cyclophilin E)
8	0.14	0.02	0.14	0.14	0.005	down	Hs.78305	Mm.21905	RAB2	RAB2, member RAS oncogene family
9	0.16	0.003	0.07	0.16	1.7E-05	up	Hs.81170	Mm.2322	PIM-1	pim-1 oncogene
10	0.16	0.16	0.10	0.12	4.8E-07	up	Hs.17778	Mm.30314	NRP2	neuropilin 2

[a]Human samples were divided into Myc-low and Myc-high groups based on their measured levels of Myc expression using method b2 (Fig. 7A, Experimental Procedures).
[b]Genes are ranked by the maximum Student's t test p value across all datasets.
[c]Up- or downregulated in Myc-high tumors. n, number of samples.
*Consistent with the design of the algorithm, Myc is at the top of the list.

cancer, *PTOV1* (prostate tumor overexpressed gene 1), or Myc function, *ID3* (inhibitor of DNA binding 3) (Lasorella et al., 2001).

Discussion

The *Myc* transgenic models of prostate cancer described here offer several advantages over current models in which the SV40 large T antigen serves as the initiating event. First, the histologic features of the mPIN and cancer lesions accurately reflect the predominant adenocarcinoma phenotype observed in human prostate cancer, with no evidence for the neuroendocrine phenotype observed in many of the T antigen models (Masumori et al., 2001; Perez-Stable et al., 1997). Second, the fact that mPIN lesions appear with essentially 100 percent penetrance and progress to invasive cancer with reliable kinetics should make this model suitable for preclinical therapeutic studies. In addition, the differences in progression time between the Lo-Myc and Hi-Myc models provides some flexibility in the design of secondary genetic mouse crosses to study the effects of complementing events. Finally, these mice show considerable improvement to the previously described Myc transgenic mouse driven by the C3 promoter. While the *Myc* transgenic mice driven by the PB and ARR_2PB promoters develop mPIN and cancer, the C3-*Myc* mouse fails to develop a similar phenotype, most likely due to inadequate transgene expression (Zhang et al., 2000b).

One notable feature of the mPIN lesions observed in our models is their rapid onset relative to the timing of transgene expression. This raises the possibility that Myc is sufficient to induce preneoplastic lesions in the mouse prostate in the absence of any secondary changes, consistent with reports of *Myc* gene amplification in human PIN lesions (Bubendorf et al., 1999; Jenkins et al., 1997; Qian et al., 1997). The latency for disease onset in other transgenic *Myc* cancer models varies widely and presumably reflects the availability of cooperating survival signals, as seen in the skin versus pancreatic islet cell models discussed previously (Pelengaris et al., 1999, 2002b). Further work with an inducible *Myc* transgene is required to directly address this question. Unfortunately, exogenously expressed hormone-regulated *Myc* fusion genes cannot be used due to confounding effects of currently available inducing agents such as tamoxifen on prostate cells.

There is optimism in the mouse modeling community that genetically engineered mouse models of human cancer will have utility in the preclinical evaluation of new anticancer agents, perhaps serving as better predictors of clinical activity in humans. We explored this question using hormone ablation therapy, a conventional treatment approach for advanced prostate cancer. The initial results establish that mPIN lesions are completely reversible whereas advanced adenocarcinomas undergo partial regression. Further studies are needed to determine if mice with residual, apparently quiescent lesions eventually relapse with full-blown hormone refractory prostate cancer. It will also be of interest to determine why these advanced lesions, unlike mPIN, are not fully reversible despite silencing of the transgene.

Another desired characteristic of mouse cancer models is that they recapitulate the molecular features of the human disease. Mouse-specific genomics tools for expression profiling allowed us to address this question using a global approach. Among the most interesting initial findings was reduced expression of Nkx3.1 in Myc-induced prostate tumors. Our immunohistochemical results clearly demonstrate that Myc expression and Nkx3.1 loss are distinct events, separated in time during the mPIN/cancer transition. Of note, our finding appears distinct from the Nkx3.1 loss associated with PTEN loss in the accompanying paper (Wu et al., 2003) where reduced Nkx3.1 expression is coincident with PTEN loss, implying coordinate regulation in a single pathway. One compelling explanation for our result is that loss of Nkx3.1 complements increased Myc expression to promote the mPIN/cancer transition. Two additional findings support this hypothesis. First, comparative genomic hybridization studies of human prostate cancer often report the parallel presence of chromosome 8q24 gain (*Myc*) and 8p22 loss (*Nkx3.1*) in the same tumor (Tsuchiya et al., 2002). Second, *Nkx3.1* knockout mice develop mPIN lesions but not cancer, suggesting that a rate-limiting second hit may be required for full-blown tumorigenesis (Abdulkadir et al., 2002; Bhatia-Gaur et al., 1999; Kim et al., 2002). Alternatively, absence of Nkx3.1 expression may be a marker for the cell of origin in the *Myc* and *PTEN* prostate cancer models and play no functional role in the transformation process. These and other hypotheses can now be tested through genetic crosses.

In addition to examining our mouse prostate cancer gene lists for known human prostate cancer orthologs, we asked whether the *Myc* prostate tumor signature can be observed in a subset of human prostate cancers. Despite current limitations due to different microarray expression profiling platforms and the limited number of orthologs represented on mouse and human chips, we were able to verify that genes correlated with *Myc* status in the mouse can be used to define *Myc*-like human tumors and that at least one of the genes most consistently associated with the *Myc* prostate tumor signature in human tumors, *Pim-1*, is consistent with our knowledge about the role of Myc in tumorigenesis. Pim-1, a serine/threonine kinase, is known to cooperate with Myc in murine lymphoma models (Moroy et al., 1991; van Lohuizen et al., 1989), and increased Pim-1 expression was recently observed in a subset of human prostate cancers and shown to correlate with poor clinical outcome (Dhanasekaran et al., 2001). Although these investigators did not determine the Myc status of these tumors, our mouse model and subsequent analysis of human microarray datasets suggest that these genes are linked in prostate and other cancers.

While our initial analysis demonstrates the utility of cross-species comparisons of global datasets, a number of steps need to be taken to realize the full potential of this approach. It will be important to standardize expression analysis platforms to provide comprehensive coverage of the mouse and human transcriptome with appropriate cataloguing of orthologs for cross comparison. In addition, human datasets must be linked to independent tissue analysis for specific molecular lesions of interest, such as *Myc* amplification or *PTEN* loss for the examples discussed here. Parallel construction of tissue arrays from tumor samples analyzed by expression microarrays will allow such experiments to be performed. Ultimately, we envision using such cross-species comparisons to validate the relevance of mouse models for human disease, to help prioritize lengthy gene lists for functional evaluation, and to extend lists of gene cohorts that segregate with a specific molecular lesion across multiple tissues.

Experimental procedures

Plasmids

The plasmids ARR_2PB-Flag-*Myc*-PAI and PB-Flag-*Myc*-PAI were constructed by ligation of the following gene fragments into the Bluescript (KS+) backbone (Stratagene). For PB-Flag-*Myc*-PAI: the poly(A) tail of the insulin receptor gene (PAI) was subcloned into the BamHI/NotI site of the bluscript KS+ multiple cloning site (MCS). The 5′ flanking promoter region (−426/+28) of the rat probasin gene was subcloned into the KpnI/EcoRV restriction sites located in the MCS. The human *Myc* c-DNA was amplified by PCR using a 5′ primer containing the BglII restriction site and the consensus sequence for the FLAG epitope (5′GGGAGATTCTCATCGCCACCATGGAC TACAAGGACGACGACGACAAGGCCATGCCCCTCAACGTTAGCTTCACC). The epitope tag was engineered to aid with immunohistochemistry; however, we were unable to detect it via Western blot (data not shown) and relied on the human-specific anti-9E10 Myc antibody (Santa Cruz) to detect transgene expression. The 3′ primer contained a BamHI restriction site for cloning purposes (3′GGGGGATCCTTACGCACAAGAGTTC CGTAGCTGTTC). After PCR amplification, the product was gel purified, digested, and filled in using the large fragment Klenow polymerase. Following gel purification, the blunt-ended product was subcloned into the EcoRV site of the bluescript KS+ PB-PAI backbone, thus generating the PB-Flag-Myc-PAI transgenic construct. The ARR_2PB-Flag-*Myc*-PAI was generated in the same way except that the ARR_2PB promoter sequence was subcloned into the KpnI/EcoRV site instead of the PB promoter. The ARR_2PB sequence contains the original probasin sequence PB (−426/+28) plus two additional androgen response elements (Zhang et al., 2000a). The completed constructs were sequenced and tested for promoter inducibility by androgen in LNCaP cells by transient transfection before microinjection into FVB ova. By transient transfection, the ARR_2PB promoter was able to confer approximately 20× higher levels of expression than the PB promoter (data not shown).

Generation of transgenic ARR_2PB-*Myc*-PAI and PB-*Myc*-PAI mice

The ARR_2PB-*Myc*-PAI and PB-*Myc*-PAI constructs were linearized with KpnI/NotI, microinjected into fertilized FVB ova, and transplanted into a pseudopregnant female (University of Irvine Transgenic Facility). Transgenic founders were screened by PCR using genomic DNA isolated from tail snips. The 5′ primer was specific to either the ARR_2PB promoter (5′ARR_2PB-CAATGTC TGTGTACAACTGCCAACTGGGATGC) or the PB promoter (5′PB-CCGGT CGACCGGAAGCTTCCACAAGTGCATTTA), and the 3′ primer for both reactions was located at the end of the *Myc* cDNA (5′TTACGCACAAGAGTTC CGTAGCTGTTC). A PCR product of 1438 base pairs was generated from the ARR_2PB-*Myc*-PAI mice and a 1774 base pair product was produced by the PB-*Myc*-PAI mice. Seven founder lines were obtained from the ARR_2PB-*Myc*-PAI construct (designated 1, 2, 4, 7, 8, 11, and 13) whereas three founders were generated with the PB-*Myc*-PAI construct (designated # 6, 9, 10). Breedings were carried out and germline transmission was obtained by four ARR_2PB-*Myc*-PAI founders (4, 7, 11, and 13) and two PB-*Myc*-PAI mice (6 and 9). These mice were bred and the offspring were aged to determine if prostate cancer developed in the transgene-positive male mice. Prostates were isolated "en block" from transgenic and wild-type mice at 2 to 12 weeks as well as at 6, 9, 12, and 16 months and cut in half along the saggital plane. Superficial and deep H&E sections were examined on the same tissue in order to document the presence/absence of mPIN, microinvasion, and invasive adenocarcinoma (described below).

Mouse dissections, tissue isolation, and castration

Urogenital organs were isolated and prostates were microdissected in a petri dish containing 10 ml of cold phosphate-buffered saline (1× PBS, Gibco-BRL 14190144) under a dissecting microscope. Adipose tissue surrounding the mouse prostates was cleared using forceps. The mouse prostate is composed of four pairs of lobes (ventral, dorsal, lateral, and anterior lobes), which were separated from the urethra using dissecting shears. One half was used to obtain protein and RNA while the other half was fixed in 10% phosphate-buffered formalin for histology (Fisher SF100-4). The liver, testes, bone from the spine, brain, kidneys, and lungs were also isolated for both histological examination as well as protein analysis to check for nonspecific expression of Myc. For castration experiments, mice were anesthetized using Isoflurane (Abbott Laboratories). The perineal region was cleaned three times with ethanol and a betadine scrub (VWR, AJ159778), and sterile dissecting shears were used to make a 4–5 mm incision in this region. Using two sterile forceps, the testes were located and a ligature was made around the testicular vessels and the tunica albugenea that encases the testes. The testes were amputated with dissecting shears and the scrotum sutured shut with 6-0 Ethilon black monofilament nylon (Ethicon Inc., 1665). A local triple antibiotic was applied over the region of the wound to facilitate healing.

Pathological and immunohistochemical data

Mice were aged to the appropriate time point and then sacrificed for dissection. The prostate tissues that were sent for histology were marked with ink on one side (the cut side), splayed, and embedded "en face" to maximize pathologic examination of each lobe. Sections were cut in the same manner on the microtome, enabling us to orient the prostatic lobes with the bladder and the seminal vesicles as a reference point. Prostates, testes, lung, liver, bone (spine), kidney, and brain were all harvested for Western blot analysis and histology. The tissues that were kept for protein analysis were homogenized using a tissue grinder in 2× SDS buffer (100 mM Tris-Hcl pH = 6.8, 200 mM DTT, 4% SDS, 20% glycerol, 50 mM B-gly-Phosphate, 1 mM NaVo4, and 40 μg/ml PMSF) and normalized for total protein via Bio-Rad assay. Tissue used for histology was fixed initially in 10% buffered formalin phosphate (Fisher SF100-4) for 8 hr followed by gentle washing in running water and finally transferred to 70% ethanol. Serial tissue sections (4 μm thick) were cut from paraffin-embedded blocks and placed on charged glass slides. H&E and masson trichrome staining were performed using standard procedures. For immunohistochemical analysis using polyclonal antibodies, the Vector Laboratories R.T.U. Vectastain Universal Elite ABC Kit (cat# PK-7200) was used, and for monoclonal antibodies, we used the Vector M.O.M. Basic Kit (BMK-2202). Briefly, sections were deparaffinized with xylene and rehydrated through graded alcohol washes followed by antigen retrieval in a pressure cooker for 30 min in sodium citrate buffer (10 mM, pH 6.0). Slides were then incubated in 0.3% hydrogen peroxide to quench endogenous horseradish peroxidase for 30 min. The slides were then blocked by incubation in normal horse serum (dilution 1:20) in 0.1 M Tris-buffered saline (pH 6.0) and subsequently incubated for 30 min with the following antibodies diluted in Tris-buffered saline: anti-synaptophysin polyclonal antibody (Dako # A0010) diluted (1:5000), anti-α smooth muscle actin monoclonal antibody (Dako # M0851) diluted (1:1000), anti-Nkx3.1 polyclonal antibody (kindly provided by Dr. Cory Abate-Shen) diluted (1:6000), anti Ki67 polyclonal antibody (Novacastra Laboratories #NCL-Ki67p) diluted (1:20,000), anti-androgen receptor polyclonal antibody (Upstate # 06-680) diluted (1:100), anti-laminin polyclonal antibody (Sigma # L-9393) diluted (1:300). Negative controls were included in each assay. Slides were then treated with biotin-labeled anti-mouse IgG and incubated with preformed avidin biotin peroxidase complex. Metal enhanced diaminobenzidine substrate was added in the presence of horseradish peroxidase, and finally, sections were counterstained with hematoxylin, dehydrated, and mounted.

TUNEL assays

TUNEL assays were performed as described in the In Situ Cell Death Detection Kit, POD from Roche. Prior to the addition of TdT enzyme, sections were deparaffinized with xylene and rehydrated through graded alcohol washes. Antigen retrieval was performed in sodium citrate buffer (10 mM, pH 6.0) by applying microwave irradiation (750 W) for 1 min. The slides where then incubated for 5 min in 3% hydrogen peroxide to quench endogenouμs horseradish peroxidase. Next, slides were immersed for 30 min at room temperature in Tris-HCl, 0.1 M, pH = 7.5 containing 3% BSA and 20% normal bovine serum. TUNEL reaction mixture containing a 1:20 dilution of TdT enzyme was added to the slides for 2 hr at 37°C in a humidified atmosphere chamber. Fifty microliters of Converter-POD was then added to each slide and incubated at 37°C for 45 min in a humidified atmosphere chamber. DAB substrate was applied for 1 min followed by counterstaining in hematoxylin.

Evaluation of the vasculature

For visualization of vessels, mice received an intravascular injection of fluorescein isothiocyanate (FITC) labeled *Lycopersicon esculentum* lectin (1 mg/kg, Vector, Burlingame, California). This lectin binds to the luminal surface of murine vasculature. Five minutes later, the animals were fixed by perfusion of 1% paraformaldehyde in phosphate-buffered saline (pH 7.3) at a pressure of 120

mm Hg using a cannula in the left ventricle. Prostates were subsequently dissected and either mounted directly on glass slides (2 month prostates) or embedded (12 month prostates) in low melting point agarose (BioWhittaker Molecular Applications, Rockland, Maine) and cut at 200 μm sections with a Vibratome (The Vibratome Company, St. Louis, Missouri). Sections were subsequently mounted onto glass slides using anti-fade media (Vectashield, Vector, Burlingame, California) in the presence of Topo3 dye (Molecular Probes, Oregon) for visualization of nuclei and examined with a BioRad1024 confocal microscope (BioRad, Hercules, California). Evaluation of vascular density was performed on a Nikon Diaphot 300 microscope equipped with a Toshiba 3CCD camera. Number of vessels per 250 μm square was obtained by using IMAGEPRO 4.0 software (Media Cybernetics, Silver Spring, Maryland). To achieve comprehensive sampling, three independent animals were evaluated per age. Ten images of 250 μm each were assessed per animal. Statistical significance was assessed by Student's t test.

Microarray measurements

Total RNA was isolated from gross prostate tissue following microdissection using the Tri-Reagent RNA Isolation Reagent (Sigma-Aldrich cat# T9424) as described by the manufacturer. Biotin-labeled cRNA was generated following Affymetrix protocols. Briefly, first strand cDNA synthesis was carried out by reverse transcribing total RNA using Superscript Reverse Transcriptase (Gibco cat# 18064-014). Second strand synthesis was performed using 10 U/μl DNA ligase (Gibco cat# 18052-019), 10 U/μl DNA Pol I (Gibco cat# 18005-025), and 2 U/μl RNase H (Gibco cat# 18021-014). Double-stranded cDNA cleanup was done using the GeneChip Sample Cleanup Module (Affymetrix cat# P/N 900371). Synthesis of biotin-labeled cRNA was carried out using the Enzo Bioarray Kit (Enzo Diagnostics Inc. cat# 42655-20) and, following fragmentation, was hybridized to Affymetrix murine chips (U74Av2).

Data analysis

Hierarchical clustering analysis was preformed using the genes with significant variation across all samples (standard deviation (σ) $>$ 2000, coefficient of variation (σ/mean) $>$ 0.05, fraction above background $>$ 0.5) (Eisen et al., 1998). To identify the most informative set of differentially expressed genes between two sets of samples, we ranked each gene by the Student's t test probability that the means of its expression values in each set are statistically distinct. We identified the UniGene identification number for as many microarray spots as possible (http://www.ncbi.nlm.nih.gov/UniGene/).

Cross-species expression module comparison algorithm

We used two methods to identify *Myc*-associated gene expression changes seen both in mouse transgenic and human prostate tumors. A schematic of our two approaches is shown in Figure 7A. We either predicted (Figure 7A, blue path) or inferred (red path) the *Myc* status of the human tumors and then compared gene expression changes between the *Myc*-like or non-*Myc*-like human tumors to the gene expression changes caused by transgenic expression of Myc in the mouse prostate.

In the first method (blue path), we predicted the *Myc*-like or non-*Myc*-like status of human tumors using a weighted gene voting prediction algorithm trained on the *Myc* transgenic data. (a) We first generated a ranked list of mouse genes differentially expressed between wild-type and *Myc* transgenic mice using the Student's t test. Each gene on this list was assigned a weighting factor (Eisen et al., 1998). (b1) We then assigned human tumors *Myc*-like or non-*Myc*-like status using a weighted gene voting prediction algorithm (Eisen et al., 1998) using the ranked and weighted mouse gene list. We identified the human orthologs for the mouse genes using the HomoloGene database (http://www.ncbi.nlm.nih.gov/HomoloGene/). Before applying the algorithm, we normalized the expression of each gene to a mean of zero and a standard deviation of one separately in the mouse dataset and each of the human datasets.

(c) We next identified and ranked using the Student's t test the genes most differentially expressed between the predicted *Myc*-like and non-*Myc*-like groups of human samples. We preformed the above steps individually for each human dataset. (d) The tops of these lists and the list of genes differentially expressed between wild-type and transgenic mouse prostates were then combined to identify the genes most consistently modulated in all datasets. To rank the genes on the combined list, we used the maximum (worst) Student's t tests p value from the individual lists.

To determine the number of genes to use in the weighted gene voting algorithm (step b1), we used a consistency requirement. This is necessary since the weighting factor is not perfect and using too many genes results in the incorporation of noise. In summary, for all possible values of n (from 1 to the total number of orthologs), we used n genes to make the *Myc*-like and non-*Myc*-like assignments. In each case, we then determined what fraction of these n genes are significantly differentially expressed ($p < 0.1$) between the two groups (i.e., the fraction of individual genes that voted consistently with the consensus [summed] vote of all n genes). Then for the final predictions, we used the value of n for which this fraction was maximal. Applying this procedure individually to each dataset, the number of genes used in the weighted gene voting algorithm ranged from 10 to 50.

Since the different human datasets were collected using different gene microarrays with different genes present, the human orthologs used in the weighted gene voting varied between datasets. It is also noteworthy that from the genes used in the predictions, chosen only by their expression patterns in the mouse data, only one (Hs.84775) ended up on the top 10 list of genes most consistently modulated in all datasets (Table 2A).

In the second method (red path), (b2) we first inferred the *Myc* status of human tumors based on their relative Myc expression levels, assigning the tumors to one of two groups, Hi-Myc or Lo-Myc, based on whether their Myc expression level was above or below the mean Myc expression level for the dataset. Again, we preformed this step individually for each human dataset. Steps c and d were then carried out as above. For human dataset C, we only used samples with similar overall microarray hybridization intensities (scale factors between 0.7 and 1.4) (Singh et al., 2002).

Acknowledgments

We wish to thank Dr. Robert Cardiff and Dr. Scott Shappell for helpful discussions on mouse prostate pathology and Dr. David Eisenberg for support and critical discussion. K.E.-Y. is supported by a fellowship grant from the California Cancer Research Program (00-00748V-20082). G.V.T. is supported by a U.S Department of Defense prostate cancer research program (DAMD17-02-1-0027) and a UCLA Prostate SPORE Career Development grant. C.L.S. is an Investigator of the Howard Hughes Medical Institute and a Doris Duke Distinguished Scientist. Work in his laboratory is also supported by grants from the National Cancer Institute and the U.S. Department of Defense.

Received: April 22, 2003
Revised: July 25, 2003
Published: September 22, 2003

References

Abdulkadir, S.A., Magee, J.A., Peters, T.J., Kaleem, Z., Naughton, C.K., Humphrey, P.A., and Milbrandt, J. (2002). Conditional loss of Nkx3.1 in adult mice induces prostatic intraepithelial neoplasia. Mol. Cell. Biol. *22*, 1495–1503.

Ahmed, N.N., Grimes, H.L., Bellacosa, A., Chan, T.O., and Tsichlis, P.N. (1997). Transduction of interleukin-2 antiapoptotic and proliferative signals via Akt protein kinase. Proc. Natl. Acad. Sci. USA *94*, 3627–3632.

Amati, B., Alevizopoulos, K., and Vlach, J. (1998). Myc and the cell cycle. Front. Biosci. *3*, D250–D268.

Bhatia-Gaur, R., Donjacour, A.A., Sciavolino, P.J., Kim, M., Desai, N., Young, P., Norton, C.R., Gridley, T., Cardiff, R.D., Cunha, G.R., et al. (1999). Roles for Nkx3.1 in prostate development and cancer. Genes Dev. *13*, 966–977.

Bowen, C., Bubendorf, L., Voeller, H.J., Slack, R., Willi, N., Sauter, G., Gasser, T.C., Koivisto, P., Lack, E.E., Kononen, J., et al. (2000). Loss of NKX3.1 expression in human prostate cancers correlates with tumor progression. Cancer Res. *60*, 6111–6115.

Bubendorf, L., Kononen, J., Koivisto, P., Schraml, P., Moch, H., Gasser, T.C., Willi, N., Mihatsch, M.J., Sauter, G., and Kallioniemi, O.P. (1999). Survey of gene amplifications during prostate cancer progression by high-through-

out fluorescence in situ hybridization on tissue microarrays. Cancer Res. *59*, 803–806.

Coller, H.A., Grandori, C., Tamayo, P., Colbert, T., Lander, E.S., Eisenman, R.N., and Golub, T.R. (2000). Expression analysis with oligonucleotide microarrays reveals that MYC regulates genes involved in growth, cell cycle, signaling, and adhesion. Proc. Natl. Acad. Sci. USA *97*, 3260–3265.

Dang, C.V. (1999). Myc target genes involved in cell growth, apoptosis, and metabolism. Mol. Cell. Biol. *19*, 1–11.

Dhanasekaran, S.M., Barrette, T.R., Ghosh, D., Shah, R., Varambally, S., Kurachi, K., Pienta, K.J., Rubin, M.A., and Chinnaiyan, A.M. (2001). Delineation of prognostic biomarkers in prostate cancer. Nature *412*, 822–826.

Eisen, M.B., Spellman, P.T., Brown, P.O., and Botstein, D. (1998). Cluster analysis and display of genome-wide expression patterns. Proc. Natl. Acad. Sci. USA *95*, 14863–14868.

Elenbaas, B., Spirio, L., Koerner, F., Fleming, M.D., Zimonjic, D.B., Donaher, J.L., Popescu, N.C., Hahn, W.C., and Weinberg, R.A. (2001). Human breast cancer cells generated by oncogenic transformation of primary mammary epithelial cells. Genes Dev. *15*, 50–65.

Elo, J.P., and Visakorpi, T. (2001). Molecular genetics of prostate cancer. Ann. Med. *33*, 130–141.

Evan, G.I., Wyllie, A.H., Gilbert, C.S., Littlewood, T.D., Land, H., Brooks, M., Waters, C.M., Penn, L.Z., and Hancock, D.C. (1992). Induction of apoptosis in fibroblasts by Myc protein. Cell *69*, 119–128.

Garabedian, E.M., Humphrey, P.A., and Gordon, J.I. (1998). A transgenic mouse model of metastatic prostate cancer originating from neuroendocrine cells. Proc. Natl. Acad. Sci. USA *95*, 15382–15387.

Gartel, A.L., and Shchors, K. (2003). Mechanisms of Myc-mediated transcriptional repression of growth arrest genes. Exp. Cell Res. *283*, 17–21.

Golub, T.R., Slonim, D.K., Tamayo, P., Huard, C., Gaasenbeek, M., Mesirov, J.P., Coller, H., Loh, M.L., Downing, J.R., Caligiuri, M.A., et al. (1999). Molecular classification of cancer: class discovery and class prediction by gene expression monitoring. Science *286*, 531–537.

Greenberg, N.M., DeMayo, F., Finegold, M.J., Medina, D., Tilley, W.D., Aspinall, J.O., Cunha, G.R., Donjacour, A.A., Matusik, R.J., and Rosen, J.M. (1995). Prostate cancer in a transgenic mouse. Proc. Natl. Acad. Sci. USA *92*, 3439–3443.

He, W.W., Sciavolino, P.J., Wing, J., Augustus, M., Hudson, P., Meissner, P.S., Curtis, R.T., Shell, B.K., Bostwick, D.G., Tindall, D.J., et al. (1997). A novel human prostate-specific, androgen-regulated homeobox gene (NKX3.1) that maps to 8p21, a region frequently deleted in prostate cancer. Genomics *43*, 69–77.

Hurlin, P.J., Foley, K.P., Ayer, D.E., Eisenman, R.N., Hanahan, D., and Arbeit, J.M. (1995). Regulation of Myc and Mad during epidermal differentiation and HPV-associated tumorigenesis. Oncogene *11*, 2487–2501.

Jain, M., Arvanitis, C., Chu, K., Dewey, W., Leonhardt, E., Trinh, M., Sundberg, C.D., Bishop, J.M., and Felsher, D.W. (2002). Sustained loss of a neoplastic phenotype by brief inactivation of MYC. Science *297*, 102–104.

Jalkut, M.W., and Reiter, R.E. (2002). Role of prostate stem cell antigen in prostate cancer research. Curr. Opin. Urol. *12*, 401–406.

Jenkins, R.B., Qian, J., Lieber, M.M., and Bostwick, D.G. (1997). Detection of Myc oncogene amplification and chromosomal anomalies in metastatic prostatic carcinoma by fluorescence in situ hybridization. Cancer Res. *57*, 524–531.

Jensen, N.A., Pedersen, K.M., Lihme, F., Rask, L., Nielsen, J.V., Rasmussen, T.E., and Mitchelmore, C. (2002). Astroglial Myc overexpression predisposes mice to primary malignant gliomas. J. Biol. Chem. *278*, 8300–8308. Published online March 7, 2003. 10.1074/jbc.M211195200.

Karlsson, A., Giuriato, S., Tang, F., Fung-Weier, J., Levan, G., and Felsher, D.W. (2003). Genomically complex lymphomas undergo sustained tumor regression upon MYC inactivation unless they acquire novel chromosomal translocations. Blood *101*, 2797–2803.

Kasper, S., Sheppard, P.C., Yan, Y., Pettigrew, N., Borowsky, A.D., Prins, G.S., Dodd, J.G., Duckworth, M.L., and Matusik, R.J. (1998). Development, progression, and androgen-dependence of prostate tumors in probasin-large T antigen transgenic mice: a model for prostate cancer. Lab. Invest. *78*, i–xv.

Kim, M.J., Bhatia-Gaur, R., Banach-Petrosky, W.A., Desai, N., Wang, Y., Hayward, S.W., Cunha, G.R., Cardiff, R.D., Shen, M.M., and Abate-Shen, C. (2002). Nkx3.1 mutant mice recapitulate early stages of prostate carcinogenesis. Cancer Res. *62*, 2999–3004.

Kim, S.J., Uehara, H., Karashima, T., Shepherd, D.L., Killion, J.J., and Fidler, I.J. (2003). Blockade of epidermal growth factor receptor signaling in tumor cells and tumor-associated endothelial cells for therapy of androgen-independent human prostate cancer growing in the bone of nude mice. Clin. Cancer Res. *9*, 1200–1210.

Lam, L.T., Pickeral, O.K., Peng, A.C., Rosenwald, A., Hurt, E.M., Giltnane, J.M., Averett, L.M., Zhao, H., Davis, R.E., Sathyamoorthy, M., et al. (2001). Genomic-scale measurement of mRNA turnover and the mechanisms of action of the anti-cancer drug flavopiridol. Genome Biol. *2*, RESEARCH0041.

Lasorella, A., Uo, T., and Iavarone, A. (2001). Id proteins at the cross-road of development and cancer. Oncogene *20*, 8326–8333.

Luo, Q., Harmon, E., Timms, B.G., and Kretzner, L. (2001). Novel expression patterns of the myc/max/mad transcription factor network in developing murine prostate gland. J. Urol. *166*, 1071–1077.

Masumori, N., Thomas, T.Z., Chaurand, P., Case, T., Paul, M., Kasper, S., Caprioli, R.M., Tsukamoto, T., Shappell, S.B., and Matusik, R.J. (2001). A probasin-large T antigen transgenic mouse line develops prostate adenocarcinoma and neuroendocrine carcinoma with metastatic potential. Cancer Res. *61*, 2239–2249.

Moroy, T., Verbeek, S., Ma, A., Achacoso, P., Berns, A., and Alt, F. (1991). E mu N- and E mu L-myc cooperate with E mu pim-1 to generate lymphoid tumors at high frequency in double-transgenic mice. Oncogene *6*, 1941–1948.

Nesbit, C.E., Tersak, J.M., and Prochownik, E.V. (1999). MYC oncogenes and human neoplastic disease. Oncogene *18*, 3004–3016.

Pelengaris, S., Littlewood, T., Khan, M., Elia, G., and Evan, G. (1999). Reversible activation of Myc in skin: induction of a complex neoplastic phenotype by a single oncogenic lesion. Mol. Cell *3*, 565–577.

Pelengaris, S., Khan, M., and Evan, G. (2002a). Myc: more than just a matter of life and death. Nat. Rev. Cancer *2*, 764–776.

Pelengaris, S., Khan, M., and Evan, G.I. (2002b). Suppression of myc-induced apoptosis in Beta cells exposes multiple oncogenic properties of myc and triggers carcinogenic progression. Cell *109*, 321–334.

Perez-Stable, C., Altman, N.H., Mehta, P.P., Deftos, L.J., and Roos, B.A. (1997). Prostate cancer progression, metastasis, and gene expression in transgenic mice. Cancer Res. *57*, 900–906.

Perou, C.M., Jeffrey, S.S., van de Rijn, M., Rees, C.A., Eisen, M.B., Ross, D.T., Pergamenschikov, A., Williams, C.F., Zhu, S.X., Lee, J.C., et al. (1999). Distinctive gene expression patterns in human mammary epithelial cells and breast cancers. Proc. Natl. Acad. Sci. USA *96*, 9212–9217.

Prendergast, G.C. (1999). Mechanisms of apoptosis by Myc. Oncogene *18*, 2967–2987.

Qian, J., Jenkins, R.B., and Bostwick, D.G. (1997). Detection of chromosomal anomalies and Myc gene amplification in the cribriform pattern of prostatic intraepithelial neoplasia and carcinoma by fluorescence in situ hybridization. Mod. Pathol. *10*, 1113–1119.

Rodriguez-Manzaneque, J.C., Lane, T.F., Ortega, M.A., Hynes, R.O., Lawler, J., and Iruela-Arispe, M.L. (2001). Thrombospondin-1 suppresses spontaneous tumor growth and inhibits activation of matrix metalloproteinase-9 and mobilization of vascular endothelial growth factor. Proc. Natl. Acad. Sci. USA *98*, 12485–12490.

Rosenwald, A., Wright, G., Wiestner, A., Chan, W.C., Connors, J.M., Campo, E., Gascoyne, R.D., Grogan, T.M., Muller-Hermelink, H.K., Smeland, E.B., et al. (2003). The proliferation gene expression signature is a quantitative integrator of oncogenic events that predicts survival in mantle cell lymphoma. Cancer Cell *3*, 185–197.

Sato, K., Qian, J., Slezak, J.M., Lieber, M.M., Bostwick, D.G., Bergstralh, E.J., and Jenkins, R.B. (1999). Clinical significance of alterations of chromosome 8 in high-grade, advanced, nonmetastatic prostate carcinoma. J. Natl. Cancer Inst. *91*, 1574–1580.

Sears, R.C., and Nevins, J.R. (2002). Signaling networks that link cell proliferation and cell fate. J. Biol. Chem. *277*, 11617–11620.

Shibata, M.A., Ward, J.M., Devor, D.E., Liu, M.L., and Green, J.E. (1996). Progression of prostatic intraepithelial neoplasia to invasive carcinoma in C3(1)/SV40 large T antigen transgenic mice: histopathological and molecular biological alterations. Cancer Res. *56*, 4894–4903.

Singh, D., Febbo, P.G., Ross, K., Jackson, D.G., Manola, J., Ladd, C., Tamayo, P., Renshaw, A.A., D'Amico, A.V., Richie, J.P., et al. (2002). Gene expression correlates of clinical prostate cancer behavior. Cancer Cell *1*, 203–209.

Thomas, R., True, L.D., Bassuk, J.A., Lange, P.H., and Vessella, R.L. (2000). Differential expression of osteonectin/SPARC during human prostate cancer progression. Clin. Cancer Res. *6*, 1140–1149.

Tsuchiya, N., Slezak, J.M., Lieber, M.M., Bergstralh, E.J., and Jenkins, R.B. (2002). Clinical significance of alterations of chromosome 8 detected by fluorescence in situ hybridization analysis in pathologic organ-confined prostate cancer. Genes Chromosomes Cancer *34*, 363–371.

Vaarala, M.H., Porvari, K., Kyllonen, A., Lukkarinen, O., and Vihko, P. (2001). The TMPRSS2 gene encoding transmembrane serine protease is overexpressed in a majority of prostate cancer patients: detection of mutated TMPRSS2 form in a case of aggressive disease. Int. J. Cancer *94*, 705–710.

van Lohuizen, M., Verbeek, S., Krimpenfort, P., Domen, J., Saris, C., Radaszkiewicz, T., and Berns, A. (1989). Predisposition to lymphomagenesis in pim-1 transgenic mice: cooperation with Myc and N-myc in murine leukemia virus-induced tumors. Cell *56*, 673–682.

van Lohuizen, M., Verbeek, S., Scheijen, B., Wientjens, E., van der Gulden, H., and Berns, A. (1991). Identification of cooperating oncogenes in E mu-myc transgenic mice by provirus tagging. Cell *65*, 737–752.

Voeller, H.J., Augustus, M., Madike, V., Bova, G.S., Carter, K.C., and Gelmann, E.P. (1997). Coding region of NKX3.1, a prostate-specific homeobox gene on 8p21, is not mutated in human prostate cancers. Cancer Res. *57*, 4455–4459.

Watnick, R.S., Cheng, Y.N., Rangarajan, A., Ince, T.A., and Weinberg, R.A. (2003). Ras modulates Myc activity to repress thrombospondin-1 expression and increase tumor angiogenesis. Cancer Cell *3*, 219–231.

Welsh, J.B., Sapinoso, L.M., Su, A.I., Kern, S.G., Wang-Rodriguez, J., Moskaluk, C.A., Frierson, H.F., Jr., and Hampton, G.M. (2001). Analysis of gene expression identifies candidate markers and pharmacological targets in prostate cancer. Cancer Res. *61*, 5974–5978.

Whitfield, M.L., Sherlock, G., Saldanha, A.J., Murray, J.I., Ball, C.A., Alexander, K.E., Matese, J.C., Perou, C.M., Hurt, M.M., Brown, P.O., and Botstein, D. (2002). Identification of genes periodically expressed in the human cell cycle and their expression in tumors. Mol. Biol. Cell *13*, 1977–2000.

Wu, X., Wu, J., Huang, J., Powell, W.C., Zhang, J., Matusik, R.J., Sangiorgi, F.O., Maxson, R.E., Sucov, H.M., and Roy-Burman, P. (2001). Generation of a prostate epithelial cell-specific Cre transgenic mouse model for tissue-specific gene ablation. Mech. Dev. *101*, 61–69.

Zhang, J., Thomas, T.Z., Kasper, S., and Matusik, R.J. (2000a). A small composite probasin promoter confers high levels of prostate-specific gene expression through regulation by androgens and glucocorticoids in vitro and in vivo. Endocrinology *141*, 4698–4710.

Zhang, X., Lee, C., Ng, P.Y., Rubin, M., Shabsigh, A., and Buttyan, R. (2000b). Prostatic neoplasia in transgenic mice with prostate-directed overexpression of the Myc oncoprotein. Prostate *43*, 278–285.